Species-specific oculomotor control tolerances explain saccadic suppression strength differences between macaques and zebrafish

Giulia Soto[1,#], Florian A. Dehmelt[1,2,#], Matthias P. Baumann[1,3,4,#], Ibrahim Tunç[1,3,5,6], Yue Yu[1,3], Tatiana Malevich[1,3], Ziad M. Hafed[1,3,*], Aristides B. Arrenberg[1,*]

[1] Werner Reichardt Centre for Integrative Neuroscience, University of Tübingen, Tübingen, Germany
[2] Current address: Medical Department, Heinrich Heine University, Duesseldorf, German
[3] Hertie Institute for Clinical Brain Research, University of Tübingen, Tübingen, Germany
[4] Current address: Sorbonne Université, INSERM, CNRS, Institut de la Vision, Paris, France
[5] Graduate Training Centre of Neuroscience, University of Tübingen, Tübingen, Germany
[6] Current address: Computational Systems Neuroscience, Institute of Zoology, University of Cologne, Cologne, Germany
* corresponding authors: aristides.arrenberg@uni-tuebingen.de, and ziad.m.hafed@cin.uni-tuebingen.de
[#] contributed equally

Summary

Active sensing necessarily requires integrating information about both self-generated movements as well as past, present, and future afferent inputs[1,2]. However, such information is inherently variable and relies, at least in part, on uncertain extrapolations. Here, using saccadic suppression[3,4] of visual sensitivity as a classic example of sensory-motor integration, we show that suppression strength in two drastically different species, macaque monkeys and zebrafish larvae, may be a direct outcome of efficient state estimation in the presence of uncontrollable sensory and motor variability. Bayesian estimator models[5] suggest that optimal saccadic suppression should rely not just on the sensory-motor information being processed, but also on the time-dependent magnitude of unexplained variability in the nervous system encoding it. In both macaques and zebrafish larvae, and using matched visual stimulation regimes across the species, we experimentally measured saccadic suppression strength in the superior colliculus (SC) of the monkeys and the homologous optic tectum (OT) of the fish. We also experimentally quantified additive and multiplicative motor noise components in the oculomotor behavior of both species, and we furthermore estimated noise in the sensory systems. We found that inter-species differences in sensory and motor noise levels and their theoretically predicted impacts on visual sensitivity are consistent with our experimentally observed differences in saccadic suppression strength between the fish and the monkeys. Because sensory and motor noise levels can reflect the amounts of available neural resources committed to a given task, our results strongly underscore the value of incorporating computational resource limits in investigating performance differences that have evolved in homologous brain areas.

Results and Discussion

When moving through the world, our brains constantly reconcile potentially conflicting information arising from sensory inputs in a changing environment and from the internal signals of our own body movements. One striking example of this non-stationary relationship between sensory and motor information is the active vision phenomenon of saccadic suppression: a brief reduction in visual sensitivity around the time of saccadic eye movements[3,4,6–10] (Figure 1A).

Saccadic suppression is a highly conserved phenomenon across a wide range of species, from zebrafish larvae[11] to rodents[9,10] and primates/humans[3,4,7,9,12,13]. However, the neural resources in these different species are very drastically different (e.g. Figures 1B-C), providing us with an ideal opportunity to understand how computational limits in different brain sizes act to quantitatively reshape what are otherwise qualitatively identical phenomena in multiple species.

Starting from a theoretical foundation, we implemented a computational model allowing parameterization of different sensory and motor noise contributions to saccadic suppression strength. Then, using matched visual stimulation paradigms (Methods), we experimentally measured saccadic suppression strength in homologous brain structures within macaque monkeys and zebrafish larvae, two species at opposite ends of the evolutionary spectrum. Our results revealed a particularly important effect of sensory noise in dictating saccadic suppression strength in the two species.

Saccadic suppression as efficient sensory-motor estimation

Eye position control can be optimized in a closed-loop system, and a recent study suggested that saccadic suppression might be caused by efficient sensory-motor estimation across rapid eye movements[5]. According to this framework (Figure 1D), a Bayesian estimator dynamically balances predictions from both sensory and motor information according to their ever-changing reliability, particularly across saccades. Uncertainty arises explicitly from four distinct sources: the sensory input (additive sensory

noise, σ_t), the dynamics of the eye plant (additive motor noise, ξ_t), the control signal itself (multiplicative motor noise, ε_t), and the relay delay of sensory signals, δt, from the retina to higher computing areas. Taking these variable sources of noise into account, specifically around the time of rapid eye movements, sensory signals are very unreliable in estimating the eye plant's instantaneous state. Thus, to optimize state estimation during saccades, sensory signals should be discounted and motor signals preferred.

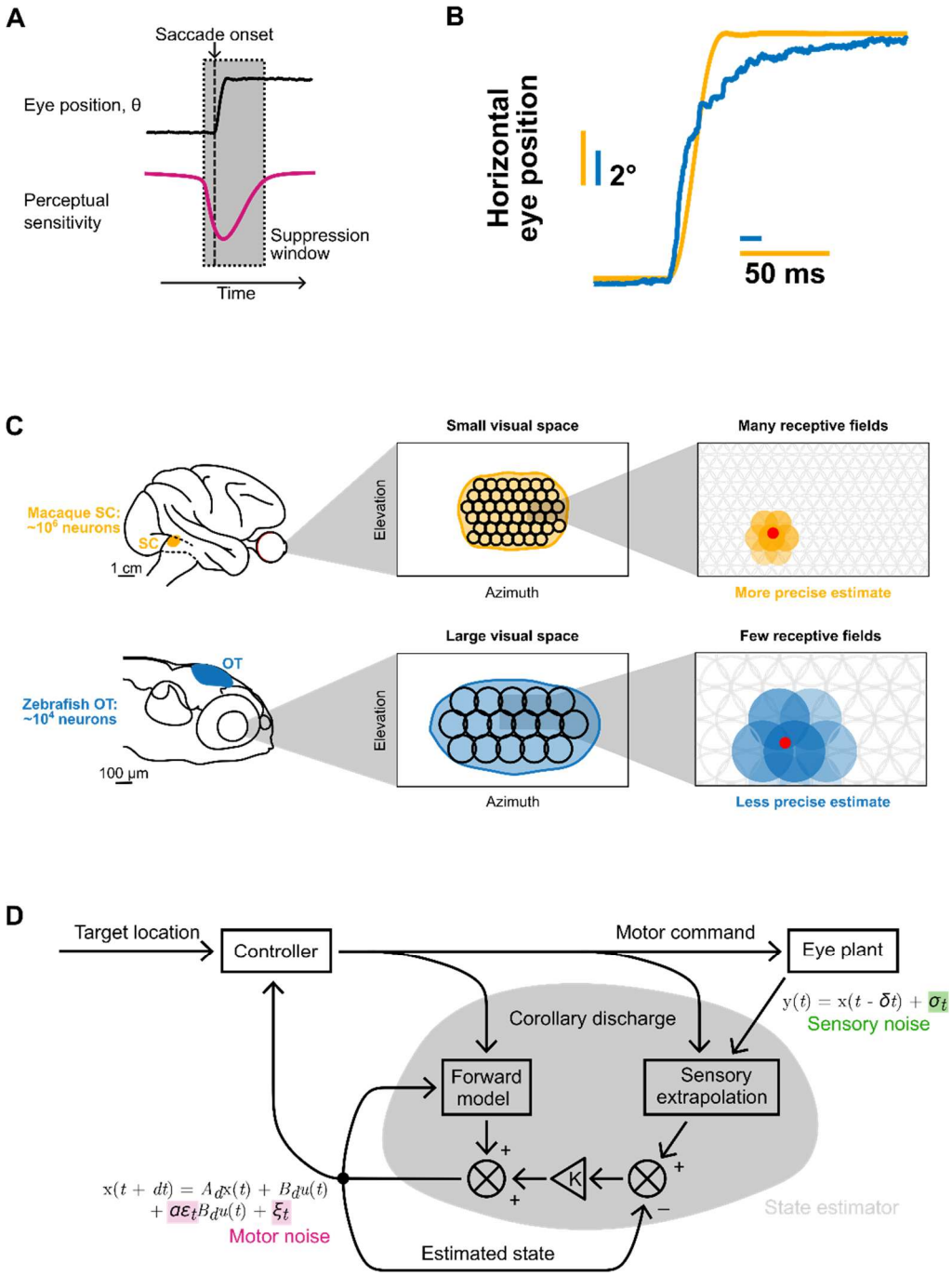

Figure 1. Saccadic suppression as efficient sensory-motor estimation.

(A) In a suppression window around the time of a saccadic eye movement, visual perceptual sensitivity to exogenous stimuli is reduced.

(B) Horizontal eye position during a saccadic eye movement of macaques (orange trace) and zebrafish (blue trace). The zebrafish saccade is executed more slowly and less accurately than the macaque saccade.

(C) Schematic linking neuronal resources to accuracy of sensory estimation in macaque and zebrafish. Macaque superior colliculus (SC) contains ~100 times as many neurons as the homologous zebrafish optic tectum (OT). This allows macaques to sample their significantly smaller visual field with many small-size receptive fields. Whereas zebrafish have to fill a larger visual field with fewer, and larger receptive fields, leading to much coarser sampling of visual space. Thus, macaques can estimate the position of a visual stimulus (red dot) more precisely than zebrafish.

(D) Schematic illustration of Bayesian state estimation for closed-loop control of eye movements (adapted from Crevecoeur and Kording[5]). To estimate the current position x of a visual target, its previous position is relayed as visual input y with delay δt and visual noise σ_t, then combined with motor activity from the corollary discharge. This extrapolation with sensory information is weighted against a purely feedforward motor extrapolation via Kálmán filter K. Eye position is moved towards this estimated target by motor control signal u with multiplicative noise ε_t, additive noise ξ_t, and a scaling factor α. A_t and B_t capture the dynamics of the eye plant, t is time, dt the time step. Changes in K correspond to saccadic suppression or enhancement. See Methods for the model and notations.).

The above mechanistic explanation of saccadic suppression relies on anatomical structures that combine sensory and motor signals. In mammals, this is found in the superior colliculus (SC), and in lower vertebrates such as zebrafish, in the optic tectum (OT)[14–18] (Figure 1C). Studies in the macaque SC and zebrafish OT have shown that saccadic suppression can indeed be observed in neurons within these structures[7,11,16,19–21], despite their large evolutionary distance from one another. Having said that, while the SC and OT are anatomically homologous, they vary vastly in size, and therefore in their ability to contribute neural resources to the optimization task required by saccadic suppression. For example, we estimated, based on brain volume and the total number of neurons in each organism, that the macaque SC has ~100 times as many neurons as the zebrafish OT (Figure 1C, Methods). Concomitantly, observations of eye position during saccadic eye movements in zebrafish and macaques (Figure 1B) revealed less accurate saccadic eye movement execution in zebrafish, indicating less precise motor control. Further, when comparing sensory accuracy (Figure 1C), we noted that zebrafish have a

much larger visual field compared to macaques, and with fewer neurons and larger receptive fields[22–24], this visual field is much more coarsely sampled in zebrafish. In summary, the zebrafish oculomotor system may have to rely on much more uncertain visual and motor information than that of macaques, particularly peri-saccadically. As we show below, this has direct implications on the strength of saccadic suppression in the two species.

Zebrafish motor signals are much noisier than those of macaques during saccadic eye movements

To assess the effect of noise levels on theoretical predictions of efficient sensory estimation, we experimentally quantified motor noise before, during, and after saccades in macaque monkeys and zebrafish (Figure 2). We recorded saccade traces (see Methods, "Noise estimation") in both species (Figures 2A and C) and estimated noise parameters for use in the model (Figures 2B, 2D). First, eye traces were split into pre-saccadic, saccadic, and post-saccadic sections (Figures 2B, 2D). Pre- and post-saccadic sections were used to determine additive motor noise, ξ, since it is modeled as independent of the motor control signal for saccades (see Methods, "Additive motor noise"). To quantify multiplicative motor noise, ε, we fit a sigmoidal curve to the saccadic section of the eye traces (Figures 2B and D). From the time derivative of the sigmoidal fit, we derived the control signal $u(t)$. A piecewise-constant approximation of $u(t)$, combined with the previously determined additive motor noise, ξ, was then used to estimate ε (see Methods, "Multiplicative motor noise"). We thus determined that zebrafish motor control is much noisier than that of macaque monkeys, with the additive motor noise being about 10 times higher in zebrafish, and the multiplicative motor noise being nearly 40 times higher (Figure 2E).

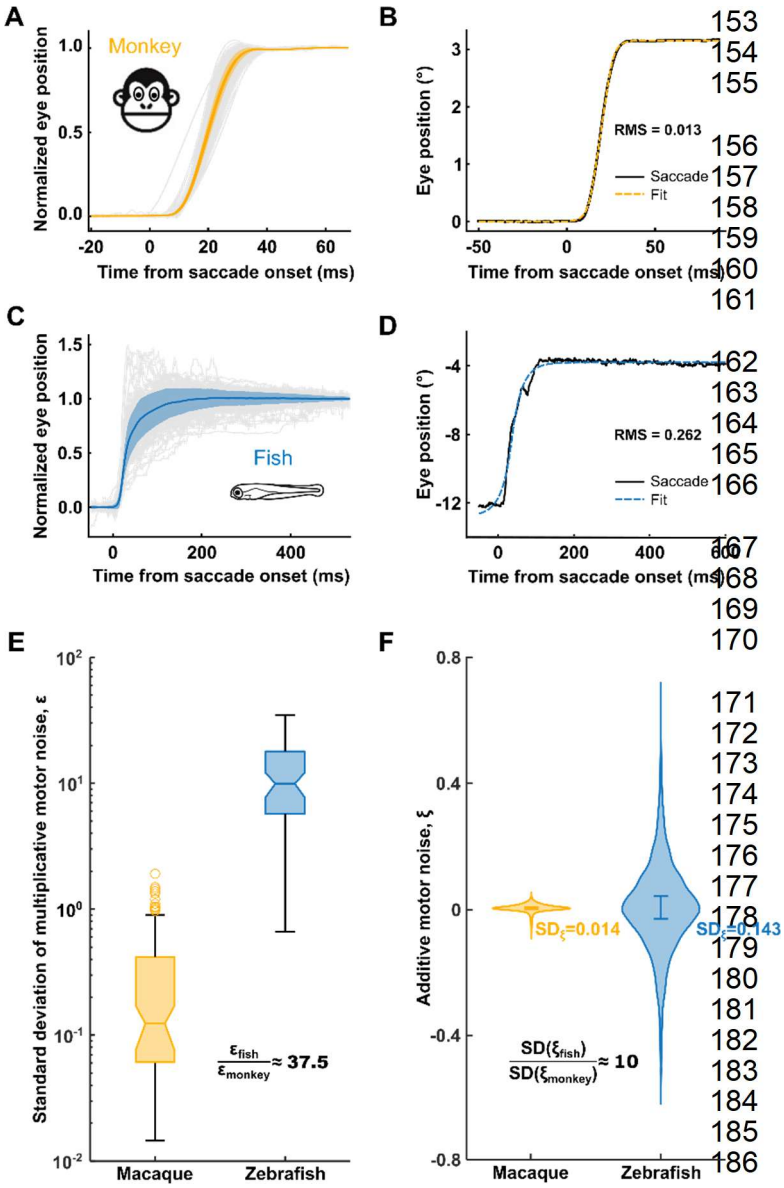

Figure 2. Zebrafish motor signals are much noisier than those of macaques during saccadic eye movements.

(A) Normalized eye position during saccadic eye movements in macaques. Grey lines indicate individual trials, colored line indicates average eye position and shaded envelope indicates standard deviation. *N = 1,445 saccades*

(B) Example macaque saccade with sigmoidal fit (dashed line). Deviations from the fit (RMS) are considered motor noise (for detailed description see STAR Methods).

(C and D) Same as (A) and (B) for zebrafish. The eye movements were much noisier than for macaques. *N = 208 saccades*

(E) Standard deviations of estimated multiplicative (ε) and additive (ξ) motor noise. Boxplot shows standard deviations of multiplicative motor noise estimates for multiple velocity bins for macaque and zebrafish during saccadic eye movement (see STAR Methods). Central line indicates median, box encloses 25th to 75th percentile and whiskers extend to minimum and maximum of data; circles show outliers. (F) Violin plot shows distribution of additive motor noise estimates pooled across all pre- and post-saccadic stationary phases for macaque and zebrafish; error bars indicate the standard deviation.

On the assumption that the precision of sensory information increases with the number of available neurons for tiling visual space, the sensory noise parameter σ for both species was then estimated from the number of neurons in their respective visual brain areas (see Methods, "Estimation of neuron count", "Sensory noise"). With about 1 million neurons in the SC and 10,000 neurons in OT, we expected the sensory noise to be 10 times larger in zebrafish compared to macaques. We were now in a position to generate predictions on saccadic suppression strength across the two species.

196 **Suppression strength differences across species are consistent with their noise**
197 **levels**

198 We first identified model parameters to reproduce the curve predicted in the original
199 study[5]. We decided to covary ξ and ε in our model; that is, we made $\varepsilon = \xi$ (Methods). This
200 was justified due to the high level of abstraction of this model, where sensory and motor
201 information are modeled as abstract variables without reference to specific neural
202 implementations. It was also further justified because across species, the ratios of
203 species' noise levels were on similar orders of magnitude for both additive (ξ) and
204 multiplicative (ε) motor noise (Figures 2E and 2F). Then, we ran further simulations in
205 which we tested the effects of varying sensory and/or motor noise by factors of up to 37.5
206 times, reflecting the inter-species noise ratios inferred in our experiments (Figures 1C,
207 2E, 2F, 3A).

208 Higher sensory noise indeed reduced the predicted optimum of saccadic suppression
209 strength, consistent with the notion that if sensory information is always unreliable, then
210 saccades have less effect on the trade-off involved in efficient state estimation (Figure
211 3B). The effect of motor noise, on the other hand, was not symmetric to that of sensory
212 noise, and noise levels observed in zebrafish primarily affected predictions of post-
213 saccadic enhancement (Figure 3C; see below and Fig. 4 for what we mean by post-
214 saccadic enhancement). This result is again congruent with our intuition when comparing
215 post-saccadic stability of eye position across the two species. Specifically, larval zebrafish
216 experience strong post saccadic drift and frequent over- and undershoots[25,26]. Therefore,
217 visual uncertainty in larval zebrafish is still high even, even after the saccade has
218 completed, thus making an enhancement of visual information immediately after the
219 saccade ineffective in zebrafish. Macaques, with much more stable post-saccadic eye
220 position (Fig. 1B), however, benefit from a brief post-saccadic enhancement. In fact,
221 snapshot enhancement, or improved feature estimation, for a brief moment immediately
222 following a saccade, has been shown in multiple biological systems[27–29]. Thus, if macaque
223 monkeys have lower sensory and motor noise than zebrafish, then the results of Figure
224 3 predict much stronger saccadic suppression, as well as post-saccadic enhancement, in
225 the monkeys than in the fish.

To test for such cross-species differences in saccadic suppression strength, we recorded neural activity in the SC of macaque monkeys and the OT of zebrafish. The visual stimulation regime for the fish was described recently[11], and it involved saccades across textured backgrounds; here we picked one of the background textures tested in the earlier study (low spatial frequency), and we directly compared it with observations from the macaque monkey data. In such data, the monkeys generated horizontal saccades (rightward or leftward across a coarse texture (Methods)). The texture was generated similarly to the fish experiments, with the only difference being that the spatial frequency ranges were matched to the receptive field sizes expected in the monkeys (Methods); this is a similar approach to our earlier multi-species comparisons of saccadic suppression[9,10].

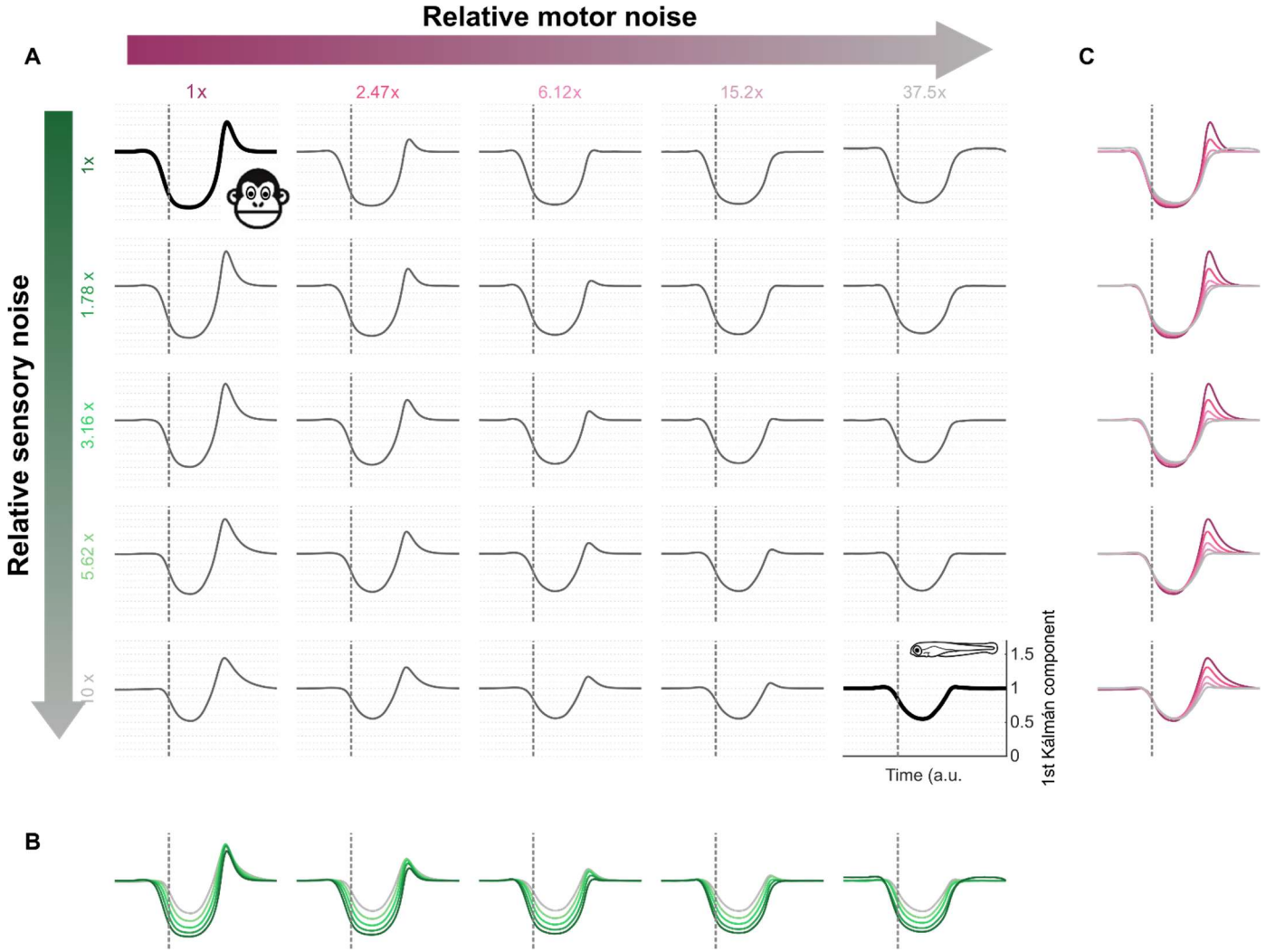

Figure 3. Bayesian estimation model predicts differences in saccadic suppression profiles across the range of noise parameters observed in macaque and zebrafish

(A) Optimal time course of saccadic suppression predicted by the model. All solid black traces show the first element of the optimal Kálmán matrix, vertical dashed lines show saccade onset. Different combinations of sensory and motor noise require different saccadic suppression. The thick trace on the upper left was obtained for macaque-like noise parameters, and the thick trace on the bottom right for zebrafish-like values. All noise parameters shown here (e.g., "10x") are relative to macaque values ("1x").

(B) Increased sensory noise reduces the depth of saccadic suppression across motor noise regimes, but in the parameter range investigated, hardly affects its overall shape. Curves are superpositions of those in the columns of (A), with shades of green indicating different magnitudes of sensory noise for the same motor noise.

(C) Increased motor noise discourages post-saccadic enhancement, and this effect is robust across sensory noise regimes. Curves are superpositions of those in the rows of (A), with shades of magenta indicating different magnitudes of motor noise for the same sensory noise.

Figures 4A and B schematically illustrate the timing of visual stimulus presentation relative to saccade onset in both species. Example neurons from the SC and OT are shown in Figures 4C and D, respectively. In both cases, responses to the flash were markedly reduced when the stimulus appeared shortly after a saccade, indicating clear saccadic suppression at the level of single units in both primates and fish. To compare suppression strength across the population, we computed cumulative distribution functions (CDFs) of suppression indices (Methods) for all included neurons (Figure 4E). The distributions revealed a clear species difference: saccadic suppression in the macaque SC was generally significantly stronger (statistical results are detailed in the legend of Fig. 4) and more prevalent than in the zebrafish OT, consistent with the model predictions (Fig. 3) that higher motor and sensory noise in zebrafish reduce the benefit of discounting sensory inputs during and immediately after saccades. Thus, while saccadic suppression is qualitatively similar in zebrafish[11] and macaque monkeys[7,16], the quantitative differences between the species can be easily reconciled by an optimization principle related to efficient state estimation under the presence of noise.

Finally, in both species, we experimentally tested visual sensitivity at multiple times relative to saccades (Methods). This allowed us to further compare the empirical data to the predictions of our model, and especially with respect to post-saccadic enhancement of visual sensitivity (Figures 4F and 4G). Specifically, for both species, the model reproduced the fact that there is always an extended time period in which visual sensitivity is reduced around saccades, regardless of suppression strength. Importantly, besides correctly predicting that saccadic suppression would be stronger in monkeys than in fish – driven solely by species-specific noise levels estimated independently (cf. Figure 2), the model also predicted that post-saccadic enhancement (Fig. 4F and Chen et al., 2017[16]) is more likely in monkeys than in fish. As mentioned above, this reflects the markedly different post-saccadic stability of eye position in the two species (Fig. 1B).

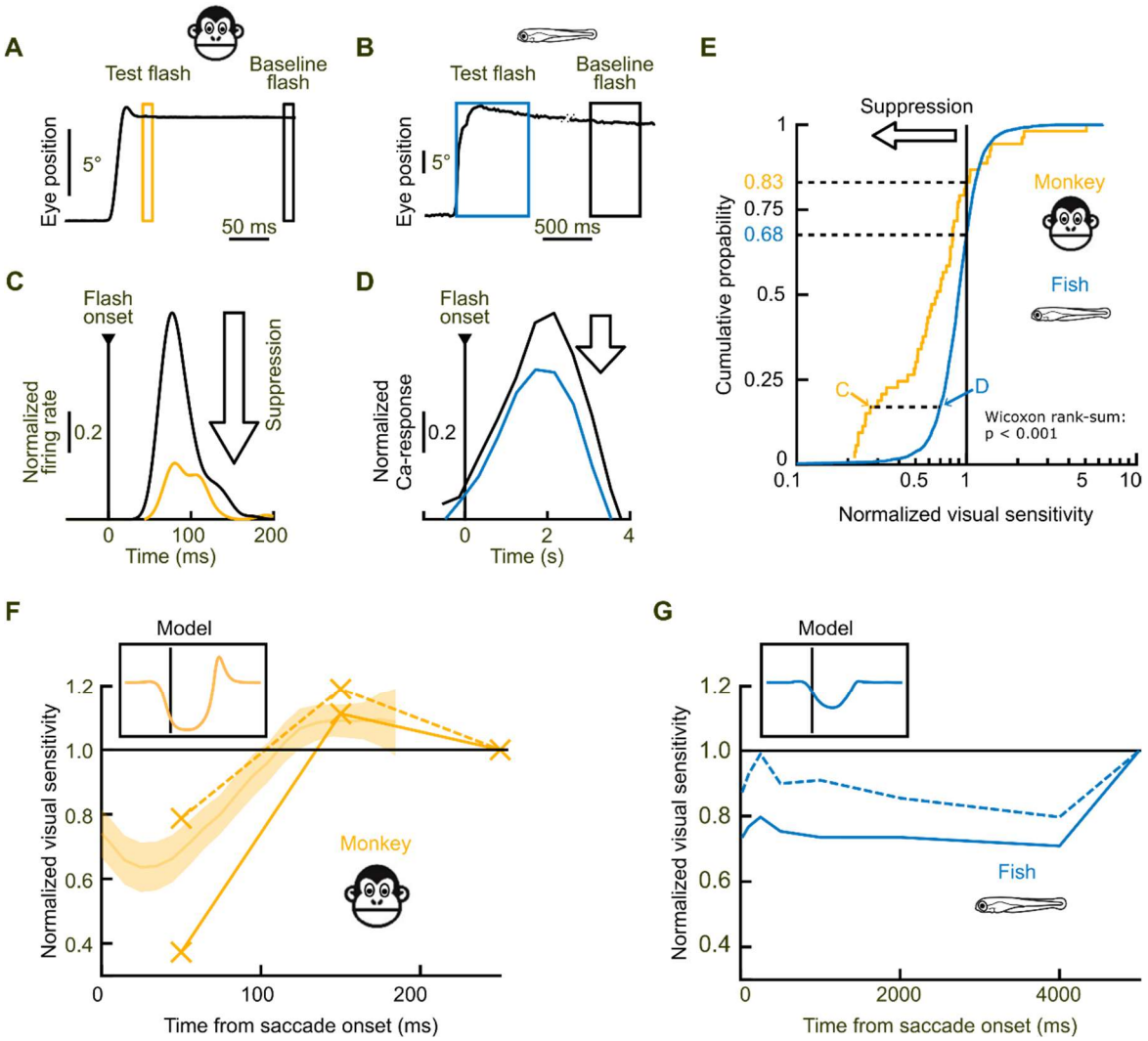

Figure 4. Saccadic suppression in the monkey superior colliculus and the zebrafish optic tectum matches model predictions.

(A) Example eye trace from a monkey with the timing of the baseline flash and a test flash ~50 ms after saccade onset, the saccade is highlighted in grey.

(B) Example eye movement trace from a zebrafish, illustrating baseline and test flash timing. Note: only a test flash 20 ms after saccade onset is shown here; in panels (D) and (E), test flashes at 20, 100, and 250 ms were pooled.

(C) Example neuron from monkey SC: visual response to the baseline flash (black) and to the test flash (orange).

(D) Example neuron from zebrafish tectum: visual response to baseline flash (black) and pooled test flashes (blue).

(E) Cumulative distribution functions of suppression strength across neurons. Example neurons from (C) and (D) are highlighted. 83% of SC neurons (orange) show suppression at 50 ms post-saccade; 68% of tectal neurons (blue) show suppression across the three tested post-saccadic times. Average suppression is stronger in SC neurons, than in tectal neurons ($p < 0.001$, Wilcoxon rank-sum test).

(F) Time course of suppression in monkey SC. Faint lines indicate data from Bellet et al. 2017[30] in which a full time course was measured; crosses show the current data from all neurons (dashed line) and the significantly suppressed ones (solid line), closely matching the Bellet et al. 2017[30] time course. Importantly, we saw systematic post-saccadic enhancement, directly consistent with the model predictions. Inset: model prediction for low sensory and motor noise, as in Figure 3A, top left.

(G) Suppression time course for zebrafish tectum neurons, analogous to (F). Inset: model prediction for high sensory and motor noise, as in Figure 3A, bottom right.

In our view, the alignment between modeling and data in our study suggests that efficient sensory-motor estimation under species-specific noise constraints provides a unifying account of saccadic suppression strength across vertebrates. We suggest that theoretical considerations of the implications of computational resource limits, like we did here, will also be valuable for our understanding of a wide range of further multi-modal, integrative brain processes.

Methods

Animal Care

All non-human primate and zebrafish experiments were evaluated by ethics committees and approved by the Tübingen regional government. For macaques we recorded SC activity from two adult, male rhesus macaque monkeys (A and F), aged 13 to 14 y and weighing 9 to 13 kg. For zebrafish we recorded calcium activity larval zebrafish 5-7 days post fertilization (dpf) with pan-neuronal GCaMP6f expression and homozygous for the *mitfa* mutation (*Tg(HuC:H2B-GCaMP6f)jf7; nacre -/-*)[31]. For eye position recordings we used 5-6 dpf larvae *nacre -/-*. Larvae were raised in E3 solution at 28°C on a 14/10 light/dark cycle.

Noise Estimation

Macaque eye position recordings

The eye data used for the noise estimation is a subset of the data published in Hafed et al., 2019[32]. It comes from the delayed saccade task, in which the monkey fixated a central spot while a peripheral target (1-degree-diameter circle) appeared and remained visible. After a variable delay (500–1,000 ms), the fixation spot disappeared, cueing a saccade to the target. We used 1,445 trials involving four oblique saccade directions with varying amplitudes. Eye data acquisition and saccade detection were performed similarly to the eprocedures described below for the current monkeys' task.

Zebrafish eye position recordings

Eye position of larval zebrafish was recorded at 1 kHz with a high-speed camera (iN8-S1 IDT, Integrated Design Tools, Inc., Pasadena, CA, USA) mounted on a stereomicroscope. Spontaneous saccades were detected using a motion trigger and 1000 frames recorded, including 200 frames pre-trigger. Recordings were manually screened for false triggers caused by non-saccadic motion within the frame and, if necessary, discarded. Eye position was extracted post-hoc using the ZebEyeTrack virtual machine[33].

Additive motor noise

Before analysis, zebrafish trials were discarded which did not meet the following criteria: both eyes move along the same direction, saccade amplitudes is greater than 5° for both eyes, and traces show no strong fluctuations for either eye. The remaining traces were visually inspected, and 5 further traces clearly showing no saccade are manually discarded. In each trial, saccade onset and offset are detected with a velocity criterion matching the variability of the eye trace[34], and trials split into pre-saccadic, saccadic, and post-saccadic periods accordingly. Additive motor noise is estimated from pre- and post-saccadic data only by fitting one affine function each to the pre- and post-saccadic traces of each trial. Deviations between best fits and raw data are interpreted as noise. We compute them for each time point, pool across trials, then compute their standard deviation to estimate ξ.

Multiplicative motor noise

Multiplicative motor noise is associated with the control signal, and thus estimated from saccadic periods under the assumption that the (previously estimated) additive motor noise remains stationary. We fit a sigmoid function to the saccadic part of each eye trace using a soft ramp[35]. As larvae occasionally show pre-saccadic drift as well as large saccadic overshoots or undershoots, and these are not the object of the present study, such trials are excluded based on fit score. The exclusion threshold is high enough to ensure that both high-noise and low-noise trials with sigmoidal saccades are included, and only significantly distorted saccades excluded. For each trial, we then computed the time derivative of the best fit to estimate control signal u, which is pooled over all eye traces. To facilitate estimation of ε, we convert u into a piecewise-constant function by dividing saccades into time bins of 100 values, computing an average $\bar{u}$ per bin, and discretizing it. Across trials, eye positions with the same discretized $\bar{u}$ are pooled; the standard deviation of their distance from best fits provides one estimate of multiplicative noise per value of $\bar{u}$. As we observed no characteristic differences between estimates obtained under high or low control signals, we averaged them to obtain ε. The arbitrary

scaling parameter α was kept at 0.06 throughout, as this allowed us to reproduce the original model results[5].

Estimation of neuron count within brain areas

Our estimation of sensory noise depended on the difference in number of neurons in primate superior colliculus versus zebrafish optic tectum. The SC of macaques has an estimated volume of 15 mm^3 (cf. Figure 3D in Chen et al., 2019[36], we used the raw data of the SC surface reconstruction). The average macaque brain has a volume of 90.000 - 100.000 mm^3 and an estimated number of 6 x 10^9 neurons[37,38]. Assuming the neuronal density to be roughly homogeneous, we multiplied the total neuron number by the fraction of SC volume relative to whole brain volume, roughly totaling 10^6 neurons. Note, however, that the homogeneous density assumption is a simplification, since subcortical structures have been reported to have lower neuron density than cortical structures[38]. 7-day-old zebrafish contain about 116,000 neurons in their entire nervous system[39]; tectal volume makes up about 8% of total nervous system volume[40]. Assuming, again, neural density to be roughly homogenous, we estimate that the tectum contains roughly 10,000 neurons. Based on our estimated neuron count and assuming, for the sake of argument, a uniform two-dimensional tiling of visual space, the 100-fold difference in neuron count translates into a difference of visual resolution on the order of $\sigma = \sqrt{100} = 10$.

Sensory Estimation Model

To model the effect of noise on efficient sensory estimation, we reconstructed a closed-loop control model that had previously been used to explain the existence and time course of saccadic suppression[5]. This abstract model treats sensory and motor information as simple 4D variables (position and velocity of eye and target, respectively), without any reference to specific neuronal implementations. In addition to our own, the original authors kindly provided unpublished MATLAB code. We manually identified parameters to reproduce the originally published time course and to improve the stability of simulations across a wider range of noise levels. Final parameters (all unitless as per the model) included $\xi \in [0.01, 0.375]$, $\sigma \in [10^{-6}, 10^{-5}]$, scaling factor $\alpha = 0.06$, sensory delay = 0.1, initial fixation time = 0.5, movement time = 0.05, stabilization time = 0.25, cost

391 function tolerance = 0.01, initial target position = -10, final target position = 20, discrete
392 time step = 0.02. Because inter-species differences were on a comparable order of
393 magnitude in both ξ (37.5x) and ε (10x), and because the effect of multiplicative motor
394 noise ε was relatively minor, we covaried the two types of motor noise in all simulations
395 reported here, with $\varepsilon = \xi$. Because of the model's high degree of abstraction, we cannot
396 directly substitute our experimentally determined noise values. Therefore, we chose an
397 approach, where we first reproduced the curve from the original modeling study[5] and then
398 multiplied the used noise levels to investigate the effects on the saccadic suppression
399 curve (Figure 3).

400 **Macaque Electrophysiology**

401 *Experimental setup*

402 The experimental setup closely followed the procedures outlined in our previous study[41].
403 In brief, experiments were conducted in a darkened room with the animal positioned
404 approximately 72 cm away from a calibrated and gamma-linearized CRT monitor
405 (covering ~30° horizontally and ~23° vertically). Stimulus presentation and data collection
406 were managed using a custom-modified version of PLDAPS[42], integrated with the
407 Psychophysics Toolbox[43] and interfaced with an OmniPlex data acquisition system
408 (Plexon, Inc.).

409 Animal preparation for behavioral training and electrophysiological recording was carried
410 out as described in earlier work[41]. Briefly, each animal was surgically implanted with a
411 head post for head stabilization and a scleral search coil in one eye[44] to enable high-
412 precision eye tracking via electromagnetic induction[45]. A recording chamber was also
413 implanted along the midline, tilted 38° posterior to vertical to target the superior colliculus.
414 We used linear multi-electrode arrays (V-Probes, Plexon Inc.) with either 20 or 24
415 channels and 50 µm inter-electrode spacing to record neuronal activity. We minimized
416 sampling bias by offline spike sorting.

Behavioral task

In each trial, monkeys performed a visually guided saccade task against a background of either a fine or a coarse texture. For each texture condition, one of 80 pre-generated images (80 fine, 80 coarse) was randomly selected and displayed as the background.

Each trial began with the presentation of a fixation spot, located 7.56° to the left or right of the screen center. After the monkey acquired and maintained fixation on this spot, it disappeared and simultaneously reappeared at the center of the screen. The monkey was trained to perform a visually guided saccade to the new (central) fixation location and to maintain gaze there for a set duration (500 ms), after which a juice reward was delivered.

During the saccade, when the eye position reached within 2.5° of the new fixation location, a probe flash was triggered. This probe, a square of size 1° × 1°, consisted of a brief luminance change (either an increase or decrease) in the pixel values of the texture at the receptive field (RF) location of the recorded superior colliculus (SC) neurons. The RFs had been previously mapped using a separate task. The receptive fields of the neurons were off the horizontal meridian, ensuring that we were measuring visual responses to peri-saccadic probes, as opposed to actual saccade-related SC motor bursts.

The flash could occur at one of three randomly chosen onset times relative to the eye crossing the 2.5° threshold: either immediately (0 ms), or with a delay of 100 ms or 200 ms. Shortly before the initial saccade onset in each trial, we calculated the fixation error and adjusted the probe position accordingly to ensure accurate alignment with the intended RF location.

Data Analysis

Eye position data were recorded at 1 kHz using scleral search coils, and neuronal activity in the superior colliculus (SC) was acquired via laminar probes. Saccades were detected offline using a previously described analysis toolbox[46], and the detected events were manually verified to ensure accuracy.

445 Spike sorting was performed offline using the Kilosort Toolbox[47], followed by manual
446 refinement with the phy software. Subsequent analyses focused on firing rates across
447 experimental conditions. Firing rates were estimated by convolving spike trains with a
448 Gaussian kernel (σ = 10 ms).

449 Only SC neurons that exhibited a significant visual response relative to baseline activity
450 (*t*-test) were included in the analysis. To quantify suppression strength, we employed an
451 analysis approach similar to that used in prior work[9].

452 First, to isolate the neural response associated with the saccade itself, we aligned spiking
453 activity to the offline-detected saccade onset and averaged responses across the portion
454 of the trial influenced by the saccade but not by the visual probe. This saccade-related
455 response was computed separately for each neuron, saccade direction, and background
456 texture condition.

457 Next, we aligned the neural activity to the onset of the probe flash and determined the
458 temporal offset between saccade onset and probe onset for each trial. The saccade-
459 related response was then temporally shifted by this offset and subtracted from the
460 individual trial activity, isolating the probe-evoked component of the response.

461 In this study, we averaged across trials in which the probe flash was either an increase
462 or a decrease in local luminance. Analysis was restricted to trials in which a coarse texture
463 served as the background.

464 To quantify the degree of suppression, we computed a suppression index for each neuron
465 by dividing the average evoked response in the 0 ms delay condition by the average
466 response in the 200 ms delay condition (baseline). The evoked response was defined as
467 the mean firing rate in the window from 50 to 200 ms after probe onset.

468 **Zebrafish *in-vivo* calcium imaging**

469 *Experimental setup*

470 Larval zebrafish were embedded in 1.6% low-melting agarose with the agarose removed
471 around the eyes to allow for free eye movements. The fish were then placed onto a

472 custom-built stage and submerged in E3 within a spherical stimulation arena, previously
473 described[11]. Visual stimuli were projected onto the surface of the stimulation arena at 60
474 Hz refresh rate at 625 nm.

475 To measure eye position, the fish were illuminated using a custom-built IR-LED ring and
476 the eyes were recorded with an infrared-filtered camera (Basler ace 2 R, a2A1920-
477 160umBAS, Basler AG, Ahrensburg, Germany) at 100 Hz. Fish were allowed to perform
478 spontaneous saccades. Eye position was extracted online and instantaneous velocity
479 computed. Saccades were detected, using a velocity threshold of at least 200°/s. To
480 optimize saccade detection, the actual velocity threshold was adjusted for each fish to
481 ensure ideal saccade detection and to avoid noise interference. To generate and display
482 visual stimuli, to extract eye position and velocity and to trigger visual stimuli in a closed-
483 loop manner we used *VxPy* (Version 0.1.4).

484 To measure calcium activity in tectal neurons we used a moveable objective two-photon
485 setup (Sutter Instruments, Novato, CA, USA) with an acquisition rate of 2.18 fps, an image
486 size of 512 x 512 pixels and a resolution of 0.88 µm x 0.88 µm per pixel. GCaMP6f was
487 excited at 920 nm and emitted light was collected using a 20x/1.0 Zeiss water immersion
488 objective.

489 *Visual stimuli*

490 Binary gaussian blur textures were displayed onto the spherical stimulation arena, as
491 previously described[11]. In response to spontaneous saccades after a delay period of 20,
492 100, 250, 500, 1000, 2000, or 4000 ms a probe flash consisting of a whole-field lumiance
493 decrease with a cosine shape, lasting 500 ms at 0.5 Hz and an amplitude of 50%
494 luminance change was displayed. To obtain a baseline response to the probe flash, it
495 was also shown 8 s after saccade detection to ensure no temporal connection between
496 saccade and probe flash.

497 *Data Analysis*

498 Calcium recordings were registered and segmented into ROIs using suite2p[48]. Further
499 analysis of registered ROIs was performed with custom-written Python (PyCharm,

500 JetBrains, Prague, Czech Republic) and Matlab (The MathWorks Inc., Natick, USA) code.
501 Fluorescence traces of individual ROIs were normalized to $\Delta F/F_0$, where F_0 was a 120
502 second sliding median window. ROIs that showed responses to the probe flash were
503 identified using regression-based analysis and only those ROIs were considered for
504 further analysis. For each ROI, saccade related responses were quantified, using control
505 conditions, where no probe flash was shown. Said saccade-related response was
506 subtracted in all other conditions during and shortly after the time of the saccade. Peak
507 $\Delta F/F_0$ responses to probe flashes were quantified and averaged for each delay condition.
508 For each ROI a suppression index for each delay was computed as in the macaque data.
509 Amongst all probe flash-responsive ROIs, truly suppressed ROIs were identified with a
510 permutation test, described previously[11].

511

References

1. Wurtz, R. H. Neuronal mechanisms of visual stability. *Vision Res.* **48**, 2070–2089 (2008).
2. Sommer, M. A. & Wurtz, R. H. Brain circuits for the internal monitoring of movements. *Annu. Rev. Neurosci.* **31**, 317 (2008).
3. Zuber, B. L. & Stark, L. Saccadic suppression: Elevation of visual threshold associated with saccadic eye movements. *Exp. Neurol.* **16**, 65–79 (1966).
4. Beeler, G. W. Visual threshold changes resulting from spontaneous saccadic eye movements. *Vision Res.* **7**, 769–775 (1967).
5. Crevecoeur, F. & Kording, K. P. Saccadic suppression as a perceptual consequence of efficient sensorimotor estimation. *Elife* **6**, (2017).
6. Bremmer, F., Kubischik, M., Hoffmann, K. P. & Krekelberg, B. Neural dynamics of saccadic suppression. *Journal of Neuroscience* **29**, 12374–12383 (2009).
7. Hafed, Z. M. & Krauzlis, R. J. Microsaccadic suppression of visual bursts in the primate superior colliculus. *Journal of Neuroscience* **30**, 9542–9547 (2010).
8. Burr, D. C., Morrone, M. C. & Ross, J. Selective suppression of the magnocellular visual pathway during saccadic eye movements. *Nature 1994 371:6497* **371**, 511–513 (1994).
9. Idrees, S., Baumann, M. P., Franke, F., Münch, T. A. & Hafed, Z. M. Perceptual saccadic suppression starts in the retina. *Nat. Commun.* **11**, 1–19 (2020).
10. Idrees, S. *et al.* Suppression without inhibition: how retinal computation contributes to saccadic suppression. *Communications Biology 2022 5:1* **5**, 1–23 (2022).
11. Soto, G. *et al.* Saccadic Suppression Enhances Saliency of Prey-Like Stimuli in the Optic Tectum. *bioRxiv* 2025.02.21.639462 (2025) doi:10.1101/2025.02.21.639462.
12. Jing Chen, X., Valsecchi, M. & Gegenfurtner, K. R. Saccadic suppression measured by steady-state visual evoked potentials. *J Neurophysiol* **122**, 251–258 (2019).
13. Zhang, Y., Valsecchi, M., Gegenfurtner, K. R. & Chen, J. The execution of saccadic eye movements suppresses visual processing of both color and luminance in the early visual cortex of humans. *J. Neurophysiol.* https://doi.org/10.1152/JN.00419.2023 (2024) doi:10.1152/JN.00419.2023.
14. Liu, X. *et al.* The Superior Colliculus: Cell Types, Connectivity, and Behavior. *Neurosci. Bull.* **38**, 1519 (2022).
15. Cang, J., Savier, E., Barchini, J. & Liu, X. Visual function, organization, and development of the mouse superior colliculus. *Annu. Rev. Vis. Sci.* **4**, 239–262 (2018).
16. Chen, C. Y. & Hafed, Z. M. A neural locus for spatial-frequency specific saccadic suppression in visual-motor neurons of the primate superior colliculus. *J. Neurophysiol.* **117**, 1657–1673 (2017).
17. Wurtz, R. H. & Albano, J. E. Visual-motor function of the primate superior colliculus. *Annu. Rev. Neurosci.* **3**, 189–226 (1980).
18. Isa, T., Marquez-Legorreta, E., Grillner, S. & Scott, E. K. The tectum/superior colliculus as the vertebrate solution for spatial sensory integration and action. *Current Biology* **31**, R741–R762 (2021).
19. Chen, C. Y., Ignashchenkova, A., Thier, P. & Hafed, Z. M. Neuronal response gain enhancement prior to microsaccades. *Current Biology* **25**, 2065–2074 (2015).

20. Wu, W. & Hafed, Z. M. Stronger premicrosaccadic sensitivity enhancement for dark contrasts in the primate superior colliculus. *Scientific Reports 2025 15:1* **15**, 1–17 (2025).
21. Hafed, Z. M., Arrenberg, A., Schwarz, C., Benda, J. & Grewe, J. Statistical regularities and the sensory consequences of self-action: A multi-species, multi-modal perspective. *Curr. Opin. Neurobiol.* **94**, 103087 (2025).
22. Easter, S. S. & Nicola, G. N. The development of vision in the zebrafish (Danio rerio). *Dev. Biol.* **180**, 646–663 (1996).
23. Rolls, E. T. & Cowey, A. Topography of the retina and striate cortex and its relationship to visual acuity in rhesus monkeys and squirrel monkeys. *Exp. Brain Res.* **10**, 298–310 (1970).
24. Schwartz, E. L. Spatial mapping in the primate sensory projection: Analytic structure and relevance to perception. *Biol. Cybern.* **25**, 181–194 (1977).
25. Brysch, C., Leyden, C. & Arrenberg, A. B. Functional architecture underlying binocular coordination of eye position and velocity in the larval zebrafish hindbrain. *BMC Biol.* **17**, 1–22 (2019).
26. Dowell, C. K., Lau, J. Y. N., Antinucci, P. & Bianco, I. H. Kinematically distinct saccades are used in a context-dependent manner by larval zebrafish. *Current Biology* **34**, 4382-4396.e5 (2024).
27. Segev, R., Schneidman, E., Goodhouse, J. & Ii, M. J. B. Role of Eye Movements in the Retinal Code for a Size Discrimination Task. *J Neurophysiol* **98**, 1380–1391 (2007).
28. Rucci, M., Iovin, R., Poletti, M. & Santini, F. Miniature eye movements enhance fine spatial detail. *Nature 2007 447:7146* **447**, 852–855 (2007).
29. Greschner, M., Bongard, M., Rujan, P. & Ammermüller, J. Retinal ganglion cell synchronization by fixational eye movements improves feature estimation. *Nature Neuroscience 2002 5:4* **5**, 341–347 (2002).
30. Bellet, J., Chen, C.-Y., Ziad, X. & Hafed, M. Sequential hemifield gating of-and-behavioral performance oscillations after microsaccades. *J Neurophysiol* **118**, 2789–2805 (2017).
31. Dunn, T. W. *et al.* Brain-wide mapping of neural activity controlling zebrafish exploratory locomotion. *Elife* **5**, (2016).
32. Hafed, Z. M. & Chen, C. Y. Sharper, Stronger, Faster Upper Visual Field Representation in Primate Superior Colliculus. *Current Biology* **26**, 1647–1658 (2016).
33. Dehmelt, F. A., Von Daranyi, A., Leyden, C. & Arrenberg, A. B. Evoking and tracking zebrafish eye movement in multiple larvae with ZebEyeTrack. *Nat. Protoc.* **13**, 1539–1568 (2018).
34. Nyström, M. & Holmqvist, K. An adaptive algorithm for fixation, saccade, and glissade detection in eyetracking data. *Behav. Res. Methods* **42**, 188–204 (2010).
35. Dai, W., Selesnick, I., Rizzo, J. R., Rucker, J. & Hudson, T. A parametric model for saccadic eye movement. *2016 IEEE Signal Processing in Medicine and Biology Symposium, SPMB 2016 - Proceedings* https://doi.org/10.1109/SPMB.2016.7846860 (2017) doi:10.1109/SPMB.2016.7846860.
36. Chen, C. Y., Hoffmann, K. P., Distler, C. & Hafed, Z. M. The Foveal Visual Representation of the Primate Superior Colliculus. *Current Biology* **29**, 2109-2119.e7 (2019).

37. Scott, J. A. *et al.* Longitudinal analysis of the developing rhesus monkey brain using magnetic resonance imaging: birth to adulthood. *Brain Struct. Funct.* **221**, 2847–2871 (2016).
38. Herculano-Houzel, S., Collins, C. E., Wong, P. & Kaas, J. H. Cellular scaling rules for primate brains. *Proc. Natl. Acad. Sci. U. S. A.* **104**, 3562–3567 (2007).
39. Petkova, M. D. *et al.* A connectomic resource for neural cataloguing and circuit dissection of the larval zebrafish brain. *bioRxiv* 2025.06.10.658982 (2025) doi:10.1101/2025.06.10.658982.
40. Shainer, I. *et al.* A single-cell resolution gene expression atlas of the larval zebrafish brain. *Sci. Adv.* **9**, eade9909 (2023).
41. Bogadhi, A. R. & Hafed, Z. M. Express detection of visual objects by primate superior colliculus neurons. *Sci. Rep.* **13**, 1–15 (2023).
42. Eastman, K. M., Huk, A. C. & Galloway, G. J. PLDAPS: A Hardware Architecture and Software Toolbox for Neurophysiology Requiring Complex Visual Stimuli and Online Behavioral Control. *Front. Neuroinform.* **6**, 14243 (2012).
43. Brainard, D. H. The Psychophysics Toolbox. *Spat. Vis.* **10**, 433–436 (1997).
44. Judge, S. J., Richmond, B. J. & Chu, F. C. Implantation of magnetic search coils for measurement of eye position: An improved method. *Vision Res.* **20**, 535–538 (1980).
45. Fuchs, A. F. & Robinson, D. A. A method for measuring horizontal and vertical eye movement chronically in the monkey. *J. Appl. Physiol.* **21**, 1068–1070 (1966).
46. Chen, C. Y. & Hafed, Z. M. Postmicrosaccadic Enhancement of Slow Eye Movements. *Journal of Neuroscience* **33**, 5375–5386 (2013).
47. Pachitariu, M., Steinmetz, N. A., Kadir, S. N., Carandini, M. & Harris, K. D. Fast and accurate spike sorting of high-channel count probes with KiloSort. *Adv. Neural Inf. Process. Syst.* **29**, (2016).
48. Pachitariu, M. *et al.* Suite2p: beyond 10,000 neurons with standard two-photon microscopy. *bioRxiv* 061507 (2017) doi:10.1101/061507.

Acknowledgements

This work was funded by the Deutsche Forschungsgemeinschaft (DFG; German Research Foundation) through the Special Priority Programme: “SPP 2205 Evolutionary optimization of neural processing” (430158665 and 430157666; AR 1076/1-2, HA 6749/3-2, AR 1076/1-1), by the Major Research Instrumentation programme of the DFG (INST 37/1254-1 FUGG), and by the Human Frontier Science Program (HFSP) Young Investigator grant RGY0079. We are grateful to Frédéric Crevecoeur of UC Louvain, Belgium, for helpful discussions of the original Bayesian estimator model, as well as for sharing some of its unpublished code.

Author Contributions

G.S. performed experiments in zebrafish optic tectum, analyzed zebrafish calcium data, generated figures, and wrote the manuscript. F.A.D. reproduced the saccadic suppression model, generated figures, and wrote the manuscript. M.P.B. performed macaque experiments, analyzed macaque eye movement data, analyzed macaque electrophysiology data, generated figures, and wrote the manuscript. I.T. analyzed zebrafish and macaque eye trace data and generated figures. Y.Y. performed macaque experiments. T.M. performed macaque experiments and analyzed macaque electrophysiology data. Z.M.H. and A.B.A. designed the overall study, acquired funding and wrote the manuscript.

Competing Interests

The authors declare no competing interests.